

# A current-driven single-atom memory

C. Schirm<sup>1†</sup>, M. Matt<sup>1</sup>, F. Pauly<sup>1</sup>, J. C. Cuevas<sup>2</sup>, P. Nielaba<sup>1</sup> and E. Scheer<sup>1\*</sup>

**The possibility of fabricating electronic devices with functional building blocks of atomic size is a major driving force of nanotechnology<sup>1</sup>. The key elements in electronic circuits are switches, usually realized by transistors, which can be configured to perform memory operations. Electronic switches have been miniaturized all the way down to the atomic scale<sup>2-9</sup>. However, at such scales, three-terminal devices are technically challenging to implement. Here we show that a metallic atomic-scale contact can be operated as a reliable and fatigue-resistant two-terminal switch. We apply a careful electromigration protocol to toggle the conductance of an aluminium atomic contact between two well-defined values in the range of a few conductance quanta. Using the nonlinearities of the current-voltage characteristics caused by superconductivity<sup>10</sup> in combination with molecular dynamics and quantum transport calculations, we provide evidence that the switching process is caused by the reversible rearrangement of single atoms. Owing to its hysteretic behaviour with two distinct states, this two-terminal switch can be used as a non-volatile information storage element.**

When the cross-section of a metal wire is reduced to a few atoms, the Fermi wavelength of the electrons becomes comparable to the contact diameter, and quantum-mechanical effects govern the electric transport properties<sup>11</sup>. As a consequence, the conductance of single-atom contacts of metals is on the order of the conductance quantum,  $G_0 = 2e^2/h \approx 77 \mu\text{S}$ , where  $e$  is the electron charge and  $h$  is the Planck constant, the exact value and distribution of the transmission probabilities of the current-carrying modes depending on the chemical valence of the metal and on the precise atomic arrangement at the constriction<sup>12</sup>. Consequently, when based on atomic motion, the implementation of functional atomic-scale building blocks such as transistors or storage devices requires the control of individual atoms in metal junctions<sup>13</sup> or of individually contacted molecules<sup>14-16</sup>. Because switches relying on the movement of individual atoms allow for potentially smaller devices than those based on larger molecules, we will concentrate here on the former.

Concepts for atomic switches include mechanical tuning<sup>17,18</sup>, bias voltage tuning<sup>13,19,20</sup> and the electrochemical approach<sup>19,21</sup>, but proof that the switching is performed by the movement of a single atom, or a few atoms, is lacking in most realizations. Similarly, two-level fluctuations in atomic-scale conductors, without stabilization in both states, have been investigated repeatedly and have been interpreted as arising from the rearrangement of single atoms or a small number of them<sup>22</sup>. Fuechsle and colleagues have recently demonstrated the single-atom function<sup>9</sup> for a several tens of nanometres sized, two-dimensional, silicon-based transistor. Electromigration is a well-established tool for thinning down mesoscopic wires to the atomic size or to produce nanometric gaps between electrode pairs of various metals<sup>23</sup>. In our proof-of-principle experiment we use electromigration-driven aluminium atomic-scale switches, because analysis of the current-voltage ( $I$ - $V$ ) characteristics of the contacts in the

superconducting state enables us to show that the high and low conductance states differ in configuration by only a very few atoms.

A few-atom aluminium contact was formed in a standard lithographic mechanically controllable break-junction<sup>10</sup> at a temperature below 1 K, as shown in Fig. 1a,b (See Methods and Supplementary Sections S1-S3 for further experimental details.). To initialize the switch, we prepared a contact with a conductance in the range of a few  $G_0$  by bending the substrate. We then ramped the bias current and monitored the linear conductance of the contact. Whenever an abrupt change of conductance (where  $\Delta G > 0.125G_0$ ) was observed, the ramp direction was reversed with a changing rate proportional to the step height. After a training period of 10 to 20 steps with irregular jump heights, a bistable situation emerged with a probability of  $\sim 15\%$ . Once the bistable situation was reached, it frequently persisted for several hours and for more than 500 switching cycles (for an example see Supplementary Section S9). Figure 1c shows the conductance response to the alternating-ramp control scheme depicted in Fig. 1d. The switching between bistable states occurs at opposite bias and at similar absolute current values  $I_s$ , with a spread of several percent. This is shown in the inset of Fig. 1c, which displays the conductance values of the main panel in the bistable situation as a function of applied current. Figure 1e summarizes further examples of bistable switches.

The switching amplitude  $\Delta G = G_H - G_L$  (where  $G_L$  and  $G_H$  are the low and high conductance values, respectively), the switching current  $I_s$  and the shape of the hysteresis loop vary from contact to contact, but typical values are  $0.2G_0 < \Delta G < 1.5G_0$  and  $10 \mu\text{A} < I_s < 50 \mu\text{A}$ . We do not find a clear preference to jump between the preferred conductance values  $G_{p1} = 0.8G_0$ ,  $G_{p2} = 1.9G_0$  and  $G_{p3} = 3.2G_0$  (known from the peaks in the aluminium conductance histogram)<sup>24</sup>. Instead, we observe a preferred jump height of  $0.3G_0$ , as summarized in the density plot of  $G_L$  versus  $G_H$  in Fig. 2. Nevertheless, there is a tendency for either  $G_H$  or  $G_L$  to correspond to one of the  $G_{pi}$ .

In principle, it could be expected that the currents required to switch from  $G_L$  to  $G_H$  and vice versa differ in size. However, their nearly identical magnitudes illustrate that the geometrical configurations of the switch are minima with a similar energy, connected by a small potential barrier. Assuming two states of very different stability, leaving the more stable one would require a large  $I_s$ . When providing this  $I_s$ , a high power would be dissipated that can trigger substantial atomic restructuring. In such a situation, it is unlikely that the junction would rearrange back to adopt the initial geometry. Hence, the bistable switching is a consequence of the chosen control scheme, which selects two states of similar stability.

To obtain insight into the geometrical arrangement in the two switch states, we analysed the  $I$ - $V$  characteristics in the superconducting state. These show nonlinearities caused by multiple Andreev reflections, which can be used to extract the transmission probabilities  $\tau_i$  of individual eigenchannels  $i$  of the atomic contacts<sup>10,12</sup>. In Fig. 3a we plot the conductance of an aluminium

<sup>1</sup>Department of Physics, University of Konstanz, D-78457 Konstanz, Germany, <sup>2</sup>Departamento de Física Teórica de la Materia Condensada and Condensed Matter Physics Center (IFIMAC), Universidad Autónoma de Madrid, E-28049 Madrid, Spain, <sup>†</sup>Present address: Astrium GmbH, 81663 Munich, Germany. \*e-mail: elke.scheer@uni-konstanz.de

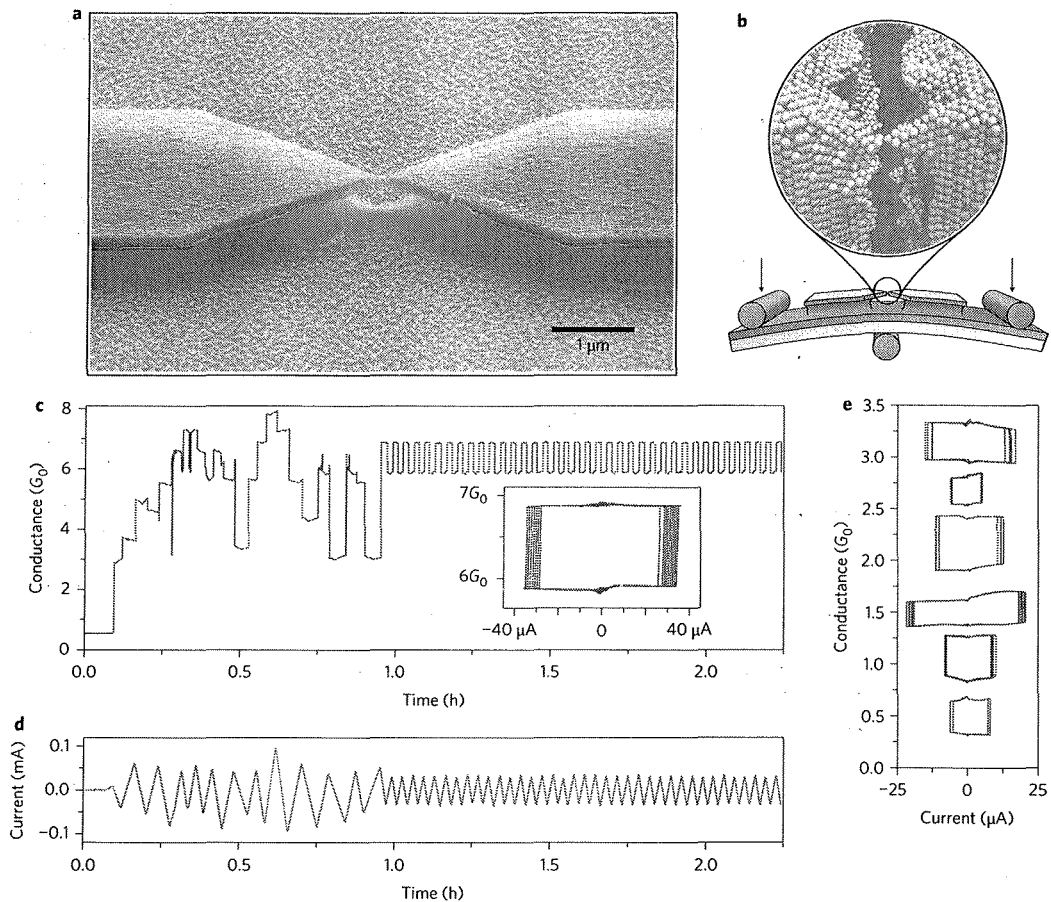


**Figure 1 | Creation of a bistable atomic switch.** **a**, Representative scanning electron microscope image (in false colours) of a break-junction sample. **b**, Principle of the break-junction set-up. A lithographically defined suspended nanobridge on a flexible substrate is elongated by bending the substrate in a three-point bending mechanism. The magnification represents an artist's view of the atomic arrangement when the nanobridge is stretched such that it forms a single-atom contact. **c**, Conductance of a break-junction structure made from aluminium as a function of time when applying the control current given in **d**. Inset: conductance versus control current for the bistable part. **d**, Control current applied for creating atomic rearrangements as a function of time. **e**, Examples of several bistable junctions plotted as a function of control current.

junction as a function of time while ramping the current. A repeated switching between two values is observed. The dotted curves in Fig. 3b are two examples of  $I$ - $V$  characteristics recorded on the high ( $G_H \approx 1.84G_0$ ) and low ( $G_L \approx 1.12G_0$ ) level of Fig. 3a. The black lines are fits to the theory of multiple Andreev reflections, revealing three channels in both the  $G_H$  and  $G_L$  states with the transmission coefficients given in the figure caption. The extracted  $\tau_i$  are also plotted in Fig. 3a, where they are assigned to the respective conductance plateau. Further switching cycles demonstrate that the distribution of the  $\tau_i$  remains unchanged in the on and off states. This proves that we reversibly switch between exactly the same two electronic states and thus between well-defined atomic configurations, because the  $\tau_i$  are much more sensitive to the atomic configuration at the constriction than for instance the total conductance that results from their sum<sup>10,25,26</sup>. In Fig. 3, all channels have non-integer transmission coefficients, characteristic of multivalent metals<sup>1,10-12,25,26</sup>, and all are affected by the reconfiguration. Further examples are given in Supplementary Section S8.

To elucidate which configurations correspond to the two states of the switch, we combined molecular dynamics simulations of the formation of atomic contacts with a tight-binding description of the electronic structure to calculate the conduction properties with the help of Green's function techniques<sup>27</sup>. We have simulated

100 stretching events for wires oriented in the  $\langle 111 \rangle$  direction to obtain a reliable statistics (see Methods and Supplementary Section S4 for further details). For a given atomic configuration, the transmission probabilities  $\tau_i$  can be calculated, but the inverse assignment is not unique. However, for a small number of open channels the number of possible stable configurations of the narrowest junction region is limited for a given set of  $\tau_i$ . Let us stress that, as we show in Supplementary Sections S6-S8, the transmission channel characteristics in the measurements for mechanically prepared contacts are similar to those for the electromigrated ones. Moreover, we show that our theory is able to reproduce the experimentally observed distributions of  $\tau_i$ . Both facts together indicate that our theory is appropriate for elucidating the atomic configurations realized by the electromigration process.

In the experiments we found that for switches operating in the range  $1G_0 - 2G_0$ , the conductance primarily changed from (i) four to three, (ii) three to three or (iii) three to two open channels. The first two pairs have also been found to be typical cases in our simulations. In Supplementary Section S8 we discuss the type (i) switching process, which involves a change in the number of channels, and show that it can be described by a transition from a configuration with two atoms at the narrowest cross-section to a dimer contact, yielding a 'two-atom switch'. Here we discuss the type (ii) process (Fig. 3),

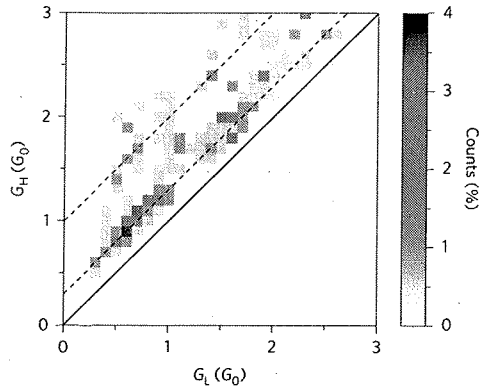


**Figure 2 |** Density plot of the counts for measuring a switch with low conductance  $G_L$  and high conductance  $G_H$ . Lines are guides to the eye, showing the diagonal (solid) and parallel (dashed) lines with offsets of  $0.3G_0$  and  $1.0G_0$ . The bin size for  $G_L$  and  $G_H$  is  $0.1G_0$ .

which can be understood as a ‘single-atom switch’. Figure 4a presents conductance versus displacement data during the stretching process. At a wire elongation of 1.5 nm a conductance jump occurs to another plateau, leaving the number of three open channels constant. The conductance of the configurations at elongations of 1.5 nm and 1.6 nm deviates by less than  $0.2G_0$  from the experimental values of  $G_H$  and  $G_L$  in Fig. 3, and the individual  $\tau_i$  also agree to within 0.2. The corresponding atomic configurations are shown in Fig. 4b,c. As one can see, the geometry changes from a single-atom contact to a dimer contact, involving the rearrangement of a single atom and the rupture of only two bonds. In Supplementary Section S8 we discuss that (within the error bounds for  $G_H$ ,  $G_L$  and  $\tau_i$  mentioned above) a similar and significant fraction of switches in both experiment and theory follow the exemplified behaviour.

It remains to clarify whether the structures found in the simulated mechanical stretching process can indeed be obtained by electromigration. Theoretical atomistic treatments of electromigration in nanometre-scale conductors are presently limited to small systems sizes (of several tens of atoms)<sup>28–30</sup>, but here we are considering contacts with around 300 dynamical atoms in the central wire. In Supplementary Section S5 we estimate that the current-induced forces during

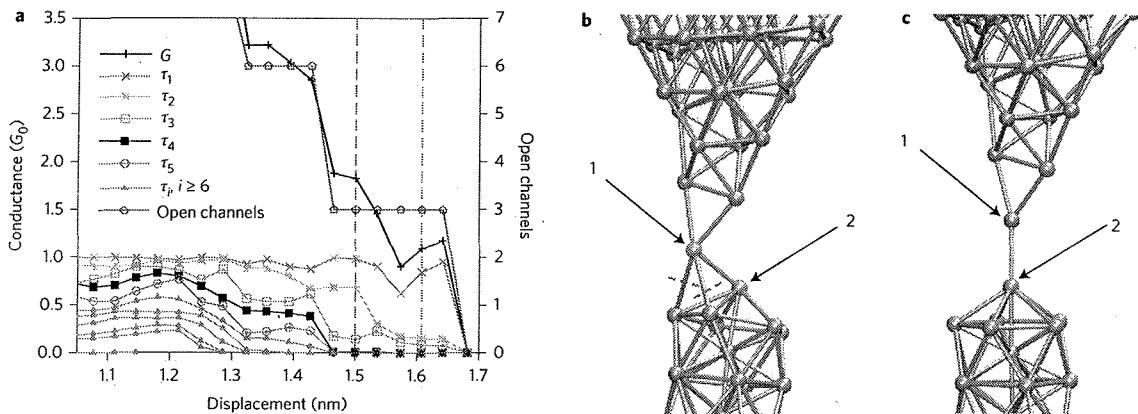


**Figure 4 |** Scenario for the switching process of Fig. 3. **a**, Theoretically determined conductance versus electrode displacement, the transmission probabilities  $\tau_i$  of the eigenchannels (left axis) and the number of open channels (right axis), a channel being counted when  $\tau_i > 0.05$ . **b,c**, Configuration of the wire at displacements of 1.50 nm (**b**) and 1.61 nm (**c**). At these points, indicated in **a** by the vertical red dashed lines, the conductance and channel transmissions in **b** are  $G = 1.83G_0$ ,  $\tau_1 = 0.99$ ,  $\tau_2 = 0.69$ ,  $\tau_3 = 0.14$  and in **c** are  $G = 1.09G_0$ ,  $\tau_1 = 0.85$ ,  $\tau_2 = 0.16$ ,  $\tau_3 = 0.09$ , similar to the experimentally observed switch in Fig. 3. The change of the positions of the atoms during the stretching process can be traced as exemplified by the atoms indicated by arrows and labelled as 1 and 2. The two red dashed lines in **b** indicate the bonds that have to be broken to cross over to the configuration shown in **c**.

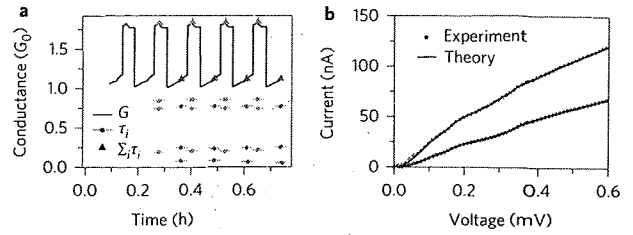


**Figure 3 |** Transmission channel analysis of a bistable switch.

**a**, Conductance versus time and its decomposition into transmission eigenchannels. The black trace is the conductance measured continuously as a function of time. Dots show the results of the superconducting  $I$ - $V$  curve-fitting procedure for  $\tau_i$  in the low conductance state with  $G_L = 1.12G_0$  (blue) and in the high conductance state with  $G_H = 1.84G_0$  (red). Red and blue triangles indicate the sum of the  $\tau_i$  and correspond well to the conductance measured directly. **b**,  $I$ - $V$  characteristics for two atomic contacts of the bistable situation shown in **a**, measured (symbols) at a temperature of  $T = 270$  mK and fit (solid lines) with the theory of multiple Andreev reflections from which we deduce channels with transmissions  $\tau_1 = 0.77$ ,  $\tau_2 = 0.24$ ,  $\tau_3 = 0.07$  (blue) and  $\tau_1 = 0.86$ ,  $\tau_2 = 0.75$ ,  $\tau_3 = 0.20$  (red).

electromigration should be sufficient to overcome the energy barriers between the two configurations of switches, as determined from our simulations of mechanical stretching. For these reasons and due to the agreement with experimental conductance values and channel transmissions, it is natural to conclude that our calculations can identify how many atoms are necessary for the switching process.

Finally, we address the operation as a memory device. Figure 5 presents a potential read-and-write scheme. After reaching a bistable situation, the control current is raised and lowered abruptly instead of ramping it continuously as before. We identify  $G_H$  with the ‘1’ state and  $G_L$  with the ‘0’ state. The bistable nature of the switch is similar to those of a flip flop. Owing to the hysteretic nature of the switching process, small current biases with short or arbitrarily long duration can be used for reading the stored information (read phase) and high negative or positive biases for changing the state (write phase). Because the conductance change is on the order of 10% or more of the absolute value, and the precision with which the states are retrieved is better than 1%, no long averaging times are necessary to detect the state.

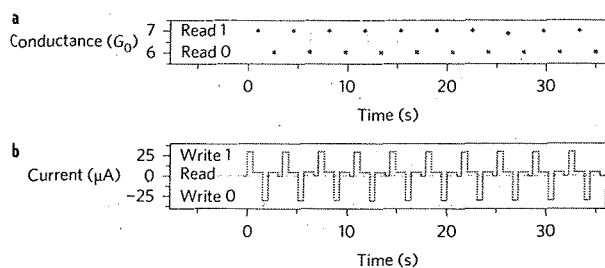


**Figure 5 | Atomic switch operated as a memory device through a stepwise variation of the current.** **a, b,** Conductance (**a**) and control current (**b**) as a function of time. At high bias currents of negative and positive sign, the switch is written into the low-conductance (0) or high-conductance (1) states, respectively. At low currents the information can be read without erasing it.

With the time resolution of our measurement set-up it was not possible to resolve the dynamics of the switching process. Because it involves the rearrangement of single atoms only, the switches are expected to be operable in the terahertz frequency range. In our case, the operation speed is limited by the time constant of the external control circuit to  $\sim 100$  kHz. To reduce the time constant, the switches could be operated in the range of  $5G_0 - 10G_0$  where the switching mechanism is still expected to be caused by the rearrangement of a few atoms.

The working principle of the two-terminal switches based on atomic contacts is not limited to aluminium. We have observed a similar switching behaviour for gold that could be implemented under ambient conditions due to its chemical inertness. For the integration of such switches into larger memory devices a crossbar technique, as demonstrated for electrochemically operated switches<sup>31</sup>, seems most promising. This implementation could pave the way for highly miniaturized storage devices.

## Methods

**Mechanically controllable break-junction technique and *I-V* measurements.** We used the standard fabrication scheme of lithographic mechanically controllable break-junctions<sup>10,11</sup> (Fig. 1). The atomic contacts were formed by uniformly bending the substrate. A pushing rod was placed at the rear side of the device close to the suspended bridge, and two counter supports ensured bending in the three-point mechanism. Specialized cryostat wiring enabled the high currents required for electromigration and provided the high-voltage resolution necessary for analysis of the *I-V* characteristics. A latching relay, operating at a temperature of  $T = 4.2$  K, was used to switch between two sets of wires. One of them exhibited a low lead resistance and was used for electromigration, while the other one was equipped with special miniaturized copper powder filters and resistive filters for absorbing the microwave radiation that would otherwise spoil the superconducting *I-V* characteristics. All transport experiments shown here were recorded in a commercial <sup>3</sup>He cryostat with a base temperature of 250 mK. Further details are provided in Supplementary Sections S1–S3.

**Computational details.** Our methodology was designed according to ref. 27. The classical molecular dynamics simulations employed semi-empirical potentials and were performed for a low temperature of  $T = 250$  mK, close to those of the transport measurements. The electrodes were separated at a speed of  $0.7 \text{ m s}^{-1}$  to simulate stretching. The electronic structure information needed for evaluation of the transmission was obtained from a Slater–Koster tight-binding description, supplemented by a local charge neutrality condition. Further details of the theoretical approach can be found in Supplementary Section S4.

Received 10 March 2013; accepted 24 July 2013;  
published online 1 September 2013

## References

1. Waser, R. *Nanoelectronics and Information Technology* (Wiley-VCH, 2003).
2. Park, J. *et al.* Coulomb blockade and the Kondo effect in single-atom transistors. *Nature* **417**, 722–725 (2002).
3. Liang, W., Shores, M. P., Bockrath, M., Long, J. R. & Park, H. Kondo resonance in a single-molecule transistor. *Nature* **417**, 725–729 (2002).
4. Kubatkin, S. *et al.* Single-electron transistor of a single organic molecule with access to several redox states. *Nature* **425**, 698–701 (2003).

5. Moth-Poulsen, K. & Bjørnholm, T. Molecular electronics with single molecules in solid-state devices. *Nature Nanotech.* **4**, 551–556 (2009).
6. Champagne, A. R., Pasupathy, A. N. & Ralph, D. C. Mechanically adjustable and electrically gated single-molecule transistors. *Nano Lett.* **5**, 305–308 (2005).
7. Martin, C. A., Smit, R. H. M., van der Zant, H. S. J. & van Ruitenbeek, J. M. A nanoelectromechanical single-atom switch. *Nano Lett.* **9**, 2940–2945 (2009).
8. Ballmann, S. & Weber, H. B. An electrostatic gate for mechanically controlled single-molecule junctions. *New J. Phys.* **14**, 123028 (2012).
9. Fuechsle, M. *et al.* A single-atom transistor. *Nature Nanotech.* **7**, 242–246 (2012).
10. Scheer, E., Joyez, P., Esteve, D., Urbina, C. & Devoret, M. H. Conduction channel transmissions of atomic-size aluminum contacts. *Phys. Rev. Lett.* **78**, 3535–3538 (1997).
11. Agrait, N., Yeyati, A. L. & van Ruitenbeek, J. M. Quantum properties of atomic-sized conductors. *Phys. Rep.* **377**, 81–279 (2003).
12. Scheer, E. *et al.* The signature of chemical valence in the electrical conduction through a single-atom contact. *Nature* **394**, 154–157 (1998).
13. Hasegawa, T., Terabe, K., Tsuruoka, T. & Aono, M. Atomic switch: atom/ion movement controlled devices for beyond von-Neumann computers. *Adv. Mater.* **24**, 252–267 (2012).
14. Van der Molen, S. J. & Liljeroth, P. Charge transport through molecular switches. *J. Phys.* **22**, 133001 (2010).
15. Miyamachi, T. *et al.* Robust spin crossover and memristance across a single molecule. *Nature Commun.* **3**, 938 (2012).
16. Quek, S. Y. *et al.* Mechanically controlled binary conductance switching of a single-molecule junction. *Nature Nanotech.* **4**, 230–234 (2009).
17. Smith, D. P. E. Quantum point contact switches. *Science* **269**, 371–373 (1995).
18. Sabater, C., Untiedt, C., Palacios, J. J. & Caturla, M. J. Mechanical annealing of metallic electrodes at the atomic scale. *Phys. Rev. Lett.* **108**, 205502 (2012).
19. Terabe, K., Hasegawa, T., Nakayama T. & Aono, M. Quantized conductance atomic switch. *Nature* **433**, 47–50 (2005).
20. Geresdi A. *et al.* From stochastic single atomic switch to nanoscale resistive memory device. *Nanoscale* **3**, 1504–1507 (2011).
21. Xie, F.-Q. *et al.* Atomic transistors with predefined quantum conductance by reversible contact reconstruction. *Nano Lett.* **8**, 4493–4497 (2008).
22. Van den Brom, H. E., Yanson, A. I. & van Ruitenbeek, J. M. Characterization of individual conductance steps in metallic quantum point contacts. *Physica B* **252**, 69–75 (1998).
23. Park, H., Lim, A. K. L., Alivisatos, A. P., Park, J. & McEuen, P. L. Fabrication of metallic electrodes with nanometer separation by electromigration. *Appl. Phys. Lett.* **75**, 301–303 (1999).
24. Yanson, I. A. & van Ruitenbeek, J. M. Do histograms constitute a proof for conductance quantization? *Phys. Rev. Lett.* **79**, 2157–2160 (1997).
25. Cuevas, J. C., Yeyati, A. L. & Martín-Rodero, A. Microscopic origin of conducting channels in metallic atomic-size contacts. *Phys. Rev. Lett.* **80**, 1066–1069 (1998).
26. Makk, P., Csonka, S. & Halbritter, A. Effect of hydrogen molecules on the electronic transport through atomic-sized metallic junctions in the superconducting state. *Phys. Rev. B* **78**, 045414 (2008).
27. Pauly, F. *et al.* Theoretical analysis of the conductance histograms and structural properties of Ag, Pt, and Ni nanocontacts. *Phys. Rev. B* **74**, 235106 (2006).
28. Todorov, T. N., Hoekstra, J. & Sutton, A. Current-induced embrittlement of atomic wires. *Phys. Rev. Lett.* **86**, 3606–3609 (2001).
29. Brandbyge, M., Stokbro, K., Taylor, J., Mozos, J.-L. & Ordejón, P. Origin of current-induced forces in an atomic gold wire: a first-principles study. *Phys. Rev. B* **67**, 193104 (2003).
30. Lü, J. T., Brandbyge, M. & Hedegård, P. Blowing the fuse: Berry's phase and runaway vibrations in molecular conductors. *Nano Lett.* **10**, 1657–1663 (2010).
31. Kuekes, P. J., Stewart, D. R. & Williams, R. S. The crossbar latch: logic value storage, restoration, and inversion in crossbar circuits. *J. Appl. Phys.* **97**, 034301 (2005).

## Acknowledgements

The authors thank H.-F. Perna for experimental assistance and M. Häfner and O. Schecker for their contributions in the early phase of this study. The authors also thank P. Leiderer for discussions. This work was supported financially by the DFG (through SFB 513 and SFB 767) and by the Baden-Württemberg Stiftung (through research network 'Functional Nanostructures'). F.P. acknowledges additional funding through the Carl Zeiss Foundation. The authors thank the NIC for computer time.

## Author contributions

C.S. performed the experiments. M.M. conducted the calculations and theoretical modelling. F.P., J.C.C., P.N. and E.S. planned the project and advised the students. All authors discussed the results and prepared the manuscript.

## Additional information

Supplementary information is available in the online version of the paper. Reprints and permissions information is available online at [www.nature.com/reprints](http://www.nature.com/reprints). Correspondence and requests for materials should be addressed to E.S.

## Competing financial interests

The authors declare no competing financial interests.